ORIGINAL RESEARCH

Parameter identification of hardening laws for bulk metal forming using experimental and numerical approach

Maxime Gruber · Nadhir Lebaal · Sebastien Roth ·
Nizar Harb · Peter Sterionow · François Peyraut

Abstract The simulative prediction of material behaviour in forming processes necessitates a precise determination of the material parameters. The present work focusses on the modelling of the isostatic part of the flow stress using a flow curve with an analytical suppression of the influence of friction and an adequate analytical law. The experimental data are obtained from isothermal upsetting tests with various upsetting ratios. The different ratios are based on a variation of the height of the sample, remaining the diameter constant. For the proposed flow stress law five parameters are identified. In order to decrease the number of function evaluations, a new reduction model method based on both analytical and sequential quadratic programming (SQP) algorithms is developed and applied to identify flow stress law parameters. A comparison with traditional SQP algorithm is also done. A 3D finite element model is built in order to simulate a side pressing test and an experimental validation is done. As numerical results fit very well experimental data, the proposed model achieves a precise prediction of the flow behaviour. The identification of the other parts of the model (i.e. dependencies on strain-rate and temperature) are conducted in further works.

Keywords Flow stress · Friction · Identification algorithm · Optimization · Finite element analysis

M. Gruber (✉) · N. Lebaal · S. Roth · N. Harb · F. Peyraut
IRTES-M3M, Belfort-Montbéliard University of Technology,
Belfort-Montbéliard, France
e-mail: maxime.gruber@utbm.fr

P. Sterionow
Institute of Metal Forming and Casting, Technische Universität
München, München, Germany

Introduction

Nowadays the use of simulative tools takes a significant part in the development process of components and production technologies. In particular process design for automotive bulk forming parts is difficult to be realized efficiently without simulative investigations. Models have to be developed to ensure a precise prediction of the process who takes into consideration the relevant effects. In the special case of forming processes, the prevision of the energy needed or of damage is one of the most relevant objectives. To get to this target, the knowledge of the flow behaviour is an important part. This behaviour can be influenced by different factors: strain, strain-rate and temperature to quote the most important ones. Those factors can be described with a constitutive law which express the flow stress of the material as a function of the considered factors.

The number of constitutive laws usable for forming processes has strongly increased over the last decades. This amount of models can be split into two categories which are the phenomenological models and the physical-based models [1]. Whereas the phenomenological models are based on the observation of the flow of metals in precise conditions, the physical-based models are related to microscopic properties of the material. Most of these models can describe dependencies of the flow stress on plastic strain, strain-rate and temperature. First the work will be focused on the dependency on plastic strain which describes the static behaviour of materials called strain hardening. The method used will be extended to strain-rate and temperature dependencies afterwards to reach the objective which is a reliable predictability of the behaviour of the part during forming processes. A recent review of important laws used in forming simulations has been performed by Lin and Chen [2].

To precisely describe the behaviour the constitutive law has to be adapted to the range of deformation that will occur in

reality. In the case of bulk forming local deformations can be extremely large. Most of the models implemented in computational codes are able to describe the flow behaviour within a limited domain of strains [3]. For the description of larger values extrapolation is usually used which makes the results uncertain and often false because the behaviour at low strains is different from the one at high strains. Bonora et al. [4] observed the strong influence of the flow law on the form of the specimen after a Taylor test. More recently, Lemoine et al. [5] used virtual experiments to study the large plastic strain levels based on hydraulic bulge test.

In the present work, experimental data is generated by performing upsetting tests of cylindrical specimens with diameter D and height H. These experimental data are used to characterize the material behaviour.

The contact between the sample and the compressive tool is of huge importance in terms of friction:

In fact the friction at the specimen-tool interface increases the force necessary for a given reduction of height so that fundamental results on the flow behaviour of the material under compressive loading cannot directly be extracted from the results. Moreover friction initiates a triaxial state of stress with a visual consequence: barrelling. The amplitude of the influence of friction on the upsetting force is directly dependent to the materials in contact described with a friction coefficient and to the upsetting ratio D/H [6]. One way to reduce the friction at the specimen-tool interface, is the use of high quality lubricants or special specimen geometries which can provide interesting results for moderate strains [7]. However, the friction is not completely suppressed by any approach and still affects the measured flow curves for large strains [8].

To neglect the influence of friction, different upsetting ratios can be used to extrapolate the results to a frictionless state with D/H=0. Cook and Larke [9] developed a methodology to extrapolate the behaviour on copper cylindrical specimens at room temperature. For high upsetting ratios D/H, the influence of friction becomes more explicit. On the opposite, very low values make the influence of friction near to negligible. Han [10] applied the extrapolation to aluminium alloys.

Based on obtained experimental data, material characterization can be conducted in order to obtain the mechanical parameters of the material to be implemented in a constitutive law. These numerical technics are widely used in the literature. Identification based on Finite Element simulation loops are possible, however the simulation time can be consequent [11]. Kim and Choi [12] used inverse analysis to predict the deformation behavior and interfacial friction under hot working conditions. A minimization of the error function

comparing experimental data and finite element simulation was conducted using gradient-based algorithms like the Golden-section search and the Broyden-Fletcher-Goldfarb-Shanno method (BFGS). Guzman et al. [13] identified the constitutive parameters of a Johnson-Cook model with temperature measurements during dynamic upsetting tests.

Finally, in this paper, experimental axial compression test were first performed with an aluminum alloy Al6082 on a SHPB apparatus. Following this step of experimental tests, numerical identification was used to calculate material parameters of three different models (Ludwik model [14], Swift [15] model, and the recent flow stress law developed by El-Magd [16]) using the sequential quadratic programming (SQP) algorithm. Two different strategies were used. The first one is based on a classical sequential quadratic programming. The second one combines SQP with a reduction of the model dimension in order to improve the convergence related to the identification process. In the literature, Harb et al. [17] used a combination between genetic algorithm (GA) and analytical optimization. The number of non-linear parameters used in the optimization is reduced, but this technique is also time-consuming because the number of evaluation of GA is very great.

Two optimization steps are conducted in this paper. Firstly the material parameters of the Ludwik, Swift and El-Magd models are identified with the calculation of the objective function by the quadratic difference between the analysed models and experimental data obtained from upsetting tests. Then we analyse if large scatter can be obtained with different models, even for the same initial flow curve and the same fitting strain range (experimental strain range).

In the second optimization study, a new flow curve is extrapolated for a large strain hardening. The same optimization approach was used to identify the material parameters of the previous models, (El-Magd, Ludwik and Swift), and a comparison between these models in terms of scatter is discussed, for the extrapolated flow curve and for the same fitting strain range (large strain range).

Then, the friction coefficient is identified by an inverse analysis fitting experimental data related to a axial test with a 3D finite element results. Finally, by using all the identified parameters inside the 3D Finite Element model (friction coefficient and material parameters of the laws), numerical replication of the side pressing test was performed for a validation step, showing an excellent correlation between the numerical and experimental values of the forging force for steel 100Cr6. The different steps of the proposed methodology are illustrated in Fig. 1.

Fig. 1 different steps of the methodology: experimental tests, parameters optimization and validation
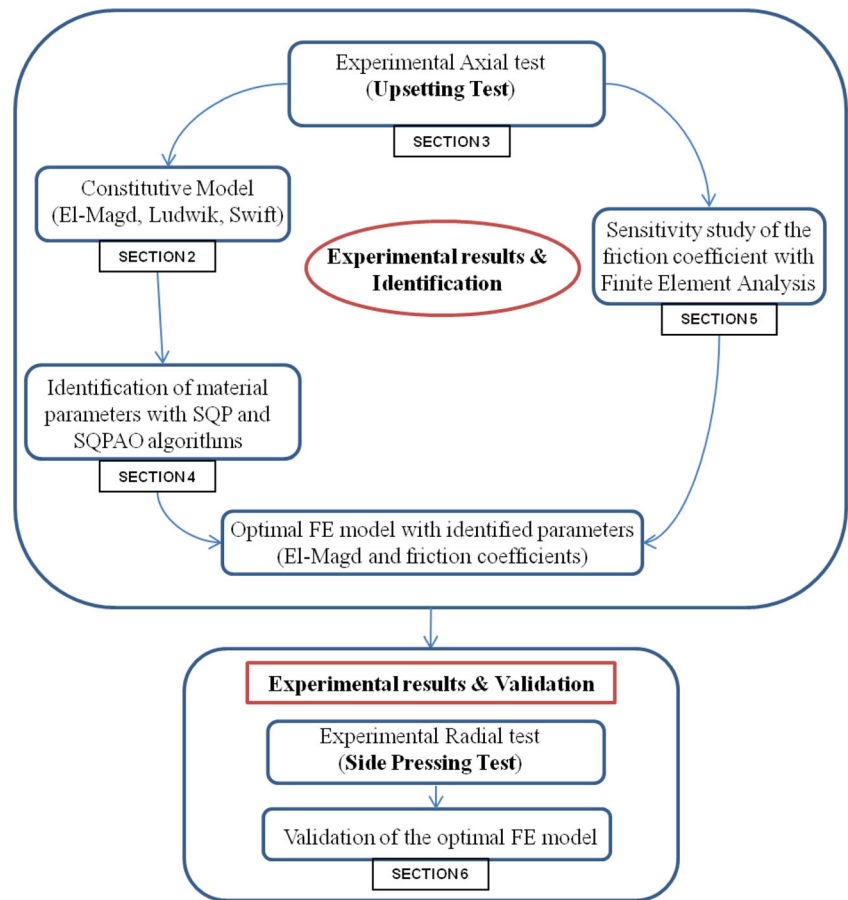
Material models

To get the most accurate description of the behaviour a theoretical model derived from the physical processes at an atomic level should be used. However, a solid theoretical approach is not available yet. In consequence semi phenomenological models are an appropriate way to do [7]. Within the present work three models will be studied. The first one, the Ludwik model, is one of the most often used in finite element codes such as Abaqus [18], Ansys [19] or LS-Dyna [20]. This model relates the stress level σ to the plastic strain level ε_p.

$$\sigma = C_1 + C_2 \varepsilon_p^n \qquad (1)$$

In this expression, C_1, C_2 and n respectively represent the yield stress, the strain hardening modulus and the strain hardening exponent of the material. The Ludwik model is used within the Johnson-Cook model to describe the static behaviour of the material [21].

The Swift model is also often used to model the material behaviour. This model introduces three constants parameters to relate the stress level σ to the plastic strain level εp as follow:

$$\sigma = C_1 \cdot \left(C_2 + \varepsilon_p \right)^n \qquad (2)$$

Where C_1, C_2 and n are material constants.

The third model that will be examined was developed by El-Magd [16] and introduces five constants for a more precise description of material flow.

$$\sigma = C_1 + C_2 \varepsilon_p + C_3 \left[1 - \exp\left(-\frac{\varepsilon_p}{C_4} \right) \right]^n \qquad (3)$$

This model showed good results for aluminium alloy AA6060 (AlMgSi0.5) and steel 42CrMo4 in the investigations of Emde [22]. This model is an extension of the Voce model [23] and combines a linear part with a coupled exponential-potential function. A similar form without the exponent n is already integrated in the finite

element code Ansys [19]. The most important advantage of this model is to consider the linear satiation of flow stress at very high plastic deformation. In fact for large strains the law will satiate to a linear curve with a slope C_2. In the case of $C_2=0$, the flow stress exhibits a maximum value.

Experimental method and materials

Extrapolation methodology

The friction has an important influence on the upsetting force. As a consequence the results obtained from an upsetting test cannot directly be used to gain the flow curve. To limit this issue, the influence of the friction has to be established in order to be able to eliminate it from the measurement results.

A basic and practical way to eliminate the influence of friction is to use different upsetting ratios D/H and to extrapolate the results to the frictionless state corresponding to a very low value of (D/H)=0 [9]. For high (large) upsetting ratios D/H, the influence of friction was found significant while very low values make the influence of friction near to negligible.

Instead of using extrapolation method, another possibility is to try to physically suppress the friction at the contact surfaces with lubrication. But usable results can only be obtained with specific specimens like the Rastegaev specimen [7]. Nevertheless, this solution was not followed in this work since such specimens do not allow to maintain the near to frictionless state for large strains [8].

To extrapolate the flow stress data obtained from experiments to suppress the influence if friction, different upsetting ratios were used. It should be taken in consideration that there is a minimal value of the D/H ratio that can be realized. In fact if the specimen becomes too slim, buckling will occur. This exhibits a minimal value of the upsetting ratio which mostly admitted to be equal to 0.4–0.5. The considered values of upsetting ratios are 0.4, 0.5, 0.67, 1.0 and 2.0. The diameter
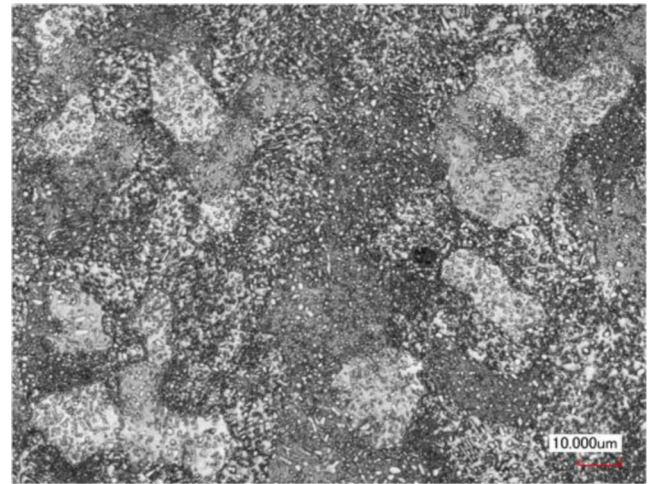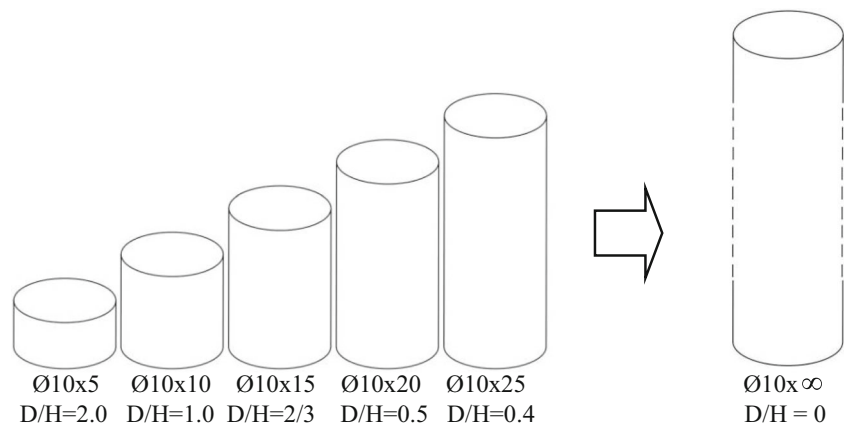

Fig. 3 Original state of the steel 1.3505 (scale 10 μm)

is kept constant and the height is varied to fit the different ratios, as illustrated in Fig. 2. All samples were machined with the same cutting conditions from the same piece of steel in order to minimize the variance due to manufacturing.

Materials

Within this paper the steel 100Cr6 will be studied. This steel is a high strength material for bearing applications [24] . The Fig. 3 shows the structure of the material before deformation. This steel has a ferritic structure with chromium carbides evenly distributed over the volume. The measured hardness is 240 HV1. The measures made on the element concentration correspond to the norm for this steel, the DIN EN ISO 683–17, see Table 1. The material is considered as isotropic.

Assuring isothermal conditions

During plastic deformation a part of the mechanical work is converted into heat [25]. If the process time is short, the heat

Fig. 2 Different sample geometries for extrapolation to infinite height

Ø10x5   Ø10x10   Ø10x15   Ø10x20   Ø10x25   Ø10x∞
D/H=2.0   D/H=1.0   D/H=2/3   D/H=0.5   D/H=0.4   D/H = 0

Table 1 Element composition of the steel 1.3505 in comparison with DIN EN ISO 683-17

Element	C	Si	Mn	P	S	Cr
Norm [%]	0,93–1,05	0,15–0,35	0,25–0,45	0–0,025	0–0,015	1,35–1,60
Samples [%]	0,985	0,302	0,342	0,0142	0,0229	1,488
Element	Mo	Al	Cu			
Norm [%]	0–0,10	0–0,05	0–0,30			
Samples [%]	0,011	0,0304	0,015			

cannot be conducted quickly enough out of the sample and temperature rises. Since the static part of the flow stress models is used for the current work, isothermal conditions have to be ensured.

In order to find the required time for isothermal case, the dimensionless Fourier number F_0 can be used [26]. It gives the time span over which the process is isothermal or adiabatic. It can be calculated as following:

$$F_0 = \frac{\alpha t}{L^2} \tag{4}$$

In this expression α, t and L are the thermal diffusivity, the process time and the characteristic dimension of the sample respectively. For the upsetting test, L is assumed to be the radius of the sample before deformation [27]. As this characteristic dimension increases, the duration of the experiment has to be increased for fully isothermal conditions. It is assumed that the process is isothermal for values of F_0 over 10. For the samples used in this paper, duration of 22 s is the minimum according to the 5 mm radius of the samples. This duration leads to a maximal initial strain rate of $\dot{\varepsilon} = 0.027 \text{ s}^{-1}$ for the smallest sample and $\dot{\varepsilon} = 0.045 \text{ s}^{-1}$ for the biggest sample. The strain rate used for all samples is $\dot{\varepsilon} = 0.01 \text{ s}^{-1}$, which corresponds to the fully isothermal domain. The velocity of the tooling is calculated based on the samples height.

Operating conditions

The upsetting test is performed within a compressive testing machine. Both dies are made of carbide with high mechanical properties to avoid permanent deformation during the upsetting test. The contact surfaces of the dies are grinded to a roughness of Rz=0.4 μm (maximum height of the profile). Figure 4 exhibits the experimental setup.

During the compression of the sample, the forging force is measured using a 600 kN "S-Type" load cell. The deformation is measured using the stroke of the upper die. Since the entire machine deforms during the testing, its stiffness is considered by measuring a load curve without any sample.

Results

As previously explained in section 3.1, a practical way to eliminate the influence of friction is to use different upsetting ratios D/H and to extrapolate the results to the frictionless state corresponding to D/H=0. The results of the upsetting tests are illustrated in Fig. 5. The total true strain ε and the true stress σ are calculated from the experimental force-displacement diagrams as followed:

$$\varepsilon = \ln\left(\frac{h}{h_0}\right) \tag{5}$$

$$\sigma = \frac{F}{S_0} \cdot \left(1 + \frac{h - h_0}{h_0}\right) \tag{6}$$

Fig. 4 Experimental setup for the upsetting tests on the universal testing machine

For both expressions, h represents the actual height of the sample, h_0 the initial height of the sample, F the actual force applied to the sample and S_0 the initial cross section of the sample. The true plastic strain ε_p can be calculated from the total true strain ε by subtracting the elastic part assuming a value of 0.2 %.

Fig. 5 Experimental flow curves for different upsetting ratios and extrapolated flow curve for steel 100Cr6
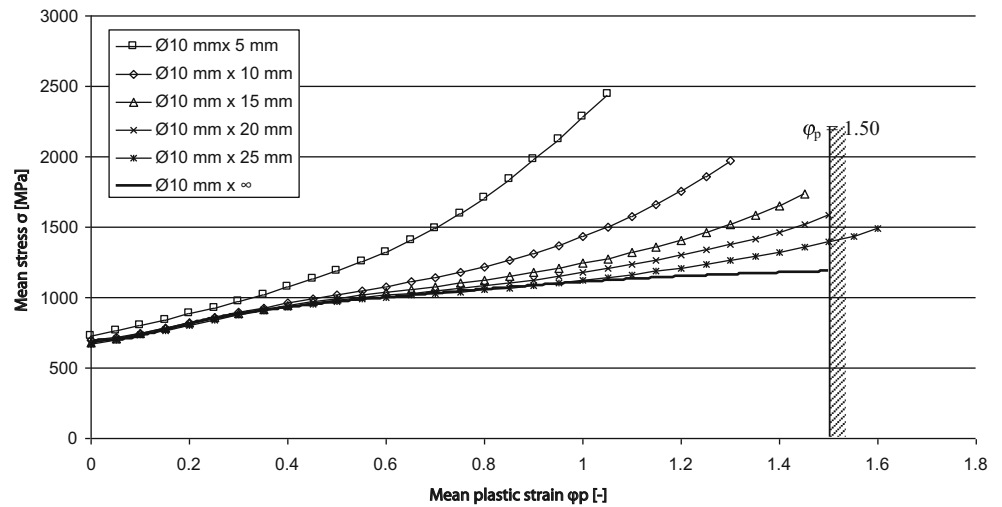
It is noted that the geometry has a great influence on the flow curve (Fig. 5). At a true plastic strain ε_p greater than 1 the value of the true flow stress σ is double for the D 10 x H 5 mm sample than for the D 10 x H 25 mm one. On the other side, the difference between sample geometries is negligible for strains below 0.2 except the D 10 x H 5 mm sample. In the case of the D 10 x H 5 mm sample, the influence of friction is strong enough to increase the measured yield strength.

For the samples with initial heights 5, 10, 15, 20 and 25 mm, the heights after upsetting are respectively 1.75, 2.78, 3.63, 4.46 and 5.15 mm.

To perform the extrapolation, the value of true flow stress σ is determined for the different upsetting ratios D/H and different true plastic strains ε_p. Then for each true plastic strain ε_p a curve of true stress σ as a function of the upsetting ratio D/H is made as illustrated in Fig. 6. In the present work, the extrapolation to D/H=0 is obtained with a second order polynomial function. Afterwards the extrapolated point is adjusted by

minimizing the first order term. Since the extrapolation is only possible when more than one experimental curve is available, the extrapolated flow curve is only built until ε_p=1.5 (Fig. 6). To summarize the results of the extrapolation, Fig. 5 illustrates the frictionless flow curves for H → ∞. For the identification of the material parameters, only the extrapolated curve without friction effect is used.

Identification of models parameters

Two optimization steps are conducted in this paper. Firstly the modelling parameters of three flow stress laws i.e. Ludwik, Swift and El-Magd are identified. A comparison between these models is conducted. in this study we analyse if large scatter can be obtained with different models, even for the same initial flow curve and the same fitting strain range

Fig. 6 Computation of the frictionless (extrapolated) flow curve for steel 100Cr6
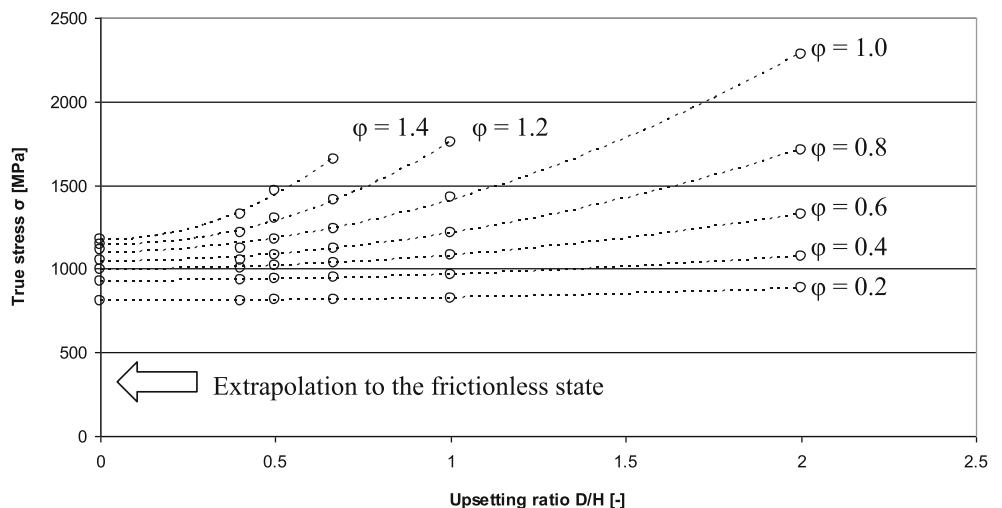
(experimental strain range). The comparison is performed only up to 1.5 strain

Experimental flow curve identification

The material parameters used in equations (1)-(3) (i.e. C_1, C_2, C_3, C_4 and n) have to be identified up to a range of true stresses and true plastic strains to predict experimental compression test. The three identification problems are formulated as the minimisation of the difference between measured data and analytical results.

$$\text{minimize} \begin{cases} J(\text{x}) = \sum_{i=1}^{m} \dfrac{(\sigma^i(\text{x}) - \sigma^i mes)^2}{\sigma^i mes} & (7) \\ \text{Such that} \quad \text{x}^l \leq \text{x} \leq \text{x}^u \end{cases}$$

$$J(\mathbf{x}) = \sum_{i=1}^{m} \frac{\left(\left(C_1 + C_2 \left(\varepsilon_p^i \right)^n \right) - \sigma_{mes}^i \right)^2}{\sigma_{mes}^i}$$

$$\Rightarrow \quad x = \begin{bmatrix} C_1 & C_2 & n \end{bmatrix} \quad \text{Ludwik's model}$$

$$J(\mathbf{x}) = \sum_{i=1}^{m} \frac{\left(\left(C_1 \cdot \left(C_2 + \varepsilon_p^i \right)^n \right) - \sigma_{mes}^i \right)^2}{\sigma_{mes}^i}$$

$$\Rightarrow \quad x = \begin{bmatrix} C_1 & C_2 & n \end{bmatrix} \text{Swift's model}$$

$$J(\mathbf{x}) = \sum_{i=1}^{m} \frac{\left[\left(C_1 + C_2 \varepsilon_p + C_3 \left[1 - \exp\left(-\frac{\varepsilon_p^i}{C_4} \right) \right]^n \right) - \sigma_{mes}^i \right]^2}{\sigma_{mes}^i}$$

$$\Rightarrow x = \begin{bmatrix} C_1 \\ C_2 \\ C_3 \\ C_4 \\ n \end{bmatrix} \text{El-Magd's model}$$

This vector is bounded by x^l and x^u which represent lower and upper limits respectively, and which are reported in Table 2, for all models. These bounded values correspond to the maximum range usually accepted for the kind of material considered in this work. It should be noticed that, for the SQP-AO strategy, only the two last variables are bounded by lower and upper limits as the three first variables are analytically calculated.

Following the approach proposed by Harb et al. in [17], it is observed for example that the El-Magd model can be expressed as follows:

$$\sigma = \begin{bmatrix} 1 & \varepsilon_p & \left(1 - \exp\left(-\frac{\varepsilon_p}{C_4} \right) \right)^n \end{bmatrix} \begin{bmatrix} C_1 \\ C_2 \\ C_3 \end{bmatrix} = N(\mathbf{x}_{nlin}) \cdot \mathbf{x}_{lin} \quad (8)$$

x_{lin} represents the linear parameters C_1, C_2 and C_3 while $N(\text{x}_{lin})$ includes the nonlinear parameters $\text{x}_{nlin} = \{C_4, n\}$.

Table 2 Lower and upper limits of optimization variables

Variables		C_1	C_2	C_3	C_4	n
Ludwik	x^l	0	−1000	–	–	0
	x^u	2000	5000	–	–	2
Swift	x^l	0	0	–	–	0
	x^u	2000	0.5	–	–	2
El-Magd	x^l	0	−1000	−5000	0.01	0
	x^u	2000	5000	1000	10	2

Where J is the objective function, $\sigma^i(x)$ and σ^i_{mes} are respectively the vectors component of calculated and measured stress and m is the number of the measured data. x is the vector of the optimization parameters. Three optimization problem which represent the identification of material parameters of Ludwik, Swift and El Magd model are resolved, the objective functions and the vectors of optimization variables are respectively represented as follows:

The combination of (7) and (8) yields to a classical least squares problem with C_1, C_2 and C_3. This problem can be analytically solved by calculating the partial derivative of $\sigma(x)$ with respect to x_{lin}

$$\mathbf{x}_{lin} = \left(N^T N \right)^{-1} N^T \sigma_{mes} \quad (9)$$

Injecting this analytical solution inside the identification process will lead to running the identification algorithm over a reduced number of two parameters C_4 and n. This space reduction can be used with any search strategy in order to minimize J(x). Gradient based approaches including BFGS (Broyden-Fletcher-Goldfarb-Shanno) and SQP (sequential quadratic programming) algorithm are among one of the earlier methods used in a non-linear optimization problem [28, 29]. In this paper, the SQP algorithm was used to solve the identification problem and search of optimal parameters. Results obtained with the reduced space minimization

Fig. 7 Convergence histories of SQP and SQPAO algorithms during the optimization run
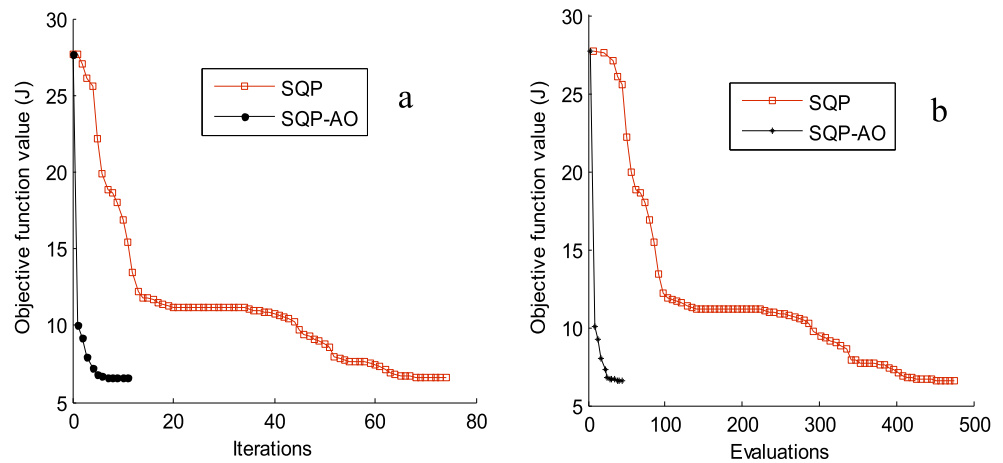
problem are labelled by SQP-AO. Those obtained with standard minimization problem are labelled SQP.

The convergence history during the optimization run is presented in Fig. 7. According to this figure it is obvious that the objective function values decreases during the optimisation iterations (Fig. 7a) and converges at the 11th and 74th iterations for SQP-AO and SQP method respectively. It can be observed in Fig. 7b that the number of function evaluations increases for the global model (SQP). This is due to the reduced number of variables (2 against 5) used by the SQP-AO method.

Table 3 presents a summary of the results obtained with the initial and optimal parameters for both optimization strategies (SQP and SQP-AO). The effect of the initial value is analysed, in terms of accuracy of the result and number of function evaluation. In order to compare the two optimization strategies, the initial values were charged and in two cases (1) and (2) the same initial value were imposed. It can be noticed that both optimization strategies give the same optimal parameters and objective function. It is also observed that the SQP-AO gives low number of function evaluation.

The same approach was also used to identify the material parameters of the other models such as Ludwik and Swift model. The optimal parameters are summarized in Table 4.

By using these identified parameters, the behaviour laws related to equations (1) (2) and (3) were compared to the experimental curve in Fig. 8. A good correlation can be observed between all models and the experimental flow curve. The relative error between identified models (El-Magd, Ludwik, and Swift) is illustrated in Fig. 9. It is observed that the relative error is less than 4 % except Ludwik model at very low values of true strain φ. It can also be noticed that El-Magd model gives the best value of the objective function, with a relative error under 1 %.

Extrapolation to large strains

According to the results obtained in [22, 23] a stress satiation can be extended beyond the limit of ε_p=1.5, as illustrated in Fig. 10. The strain hardening slope $\delta\sigma/\delta\varepsilon_p$ exhibits clearly an exponential decrease. This point leads to extrapolate the strain

Table 3 Optimization results for steel 1.3505, using SQP and SQPAO algorithm – El Magd model

Variables		C_1	C_2	C_3	C_4	n	Evaluations		J
Initial values	(1)	706	−26	658	1	1	–		27
	(2)	742	−63	587	0.5	2	–		215
	(3)	500	500	500	0.5	2	–		18112
	(4)	500	500	500	0.1	2	–		34505
Optimal values (SQP-AO)		641	158	320	0.314	1.11	(1)	44	6.63
							(2)	39	
							(3)	–	
							(4)	–	
Optimal values (SQP)		641	158	320	0.314	1.11	(1)	475	6.63
							(2)	382	
							(3)	413	
							(4)	505	

Table 4 Optimization results for El Magd, Ludwik, and Swift models - steel 1.3505

Variables	C_1	C_2	C_3	C_4	n	J
El-Magd	641	158	320	0.314	1.11	6.63
Ludiwik	559	542	–	–	0.449	53.17
Swift	1086	0.077	–	–	0.22	16.48

hardening with an exponential function (represented on Fig. 10 with square symbol). The true stress values are next approximated according to following integration formula:

$$f\left(\varepsilon_p + \Delta\varepsilon_p\right) = f\left(\varepsilon_p\right) + \Delta\varepsilon_p \cdot f'\left(\varepsilon_p\right) \qquad (10)$$

The fitting results strongly depend on the strain range chosen for the fitting. Such discrepancies between experimental and fitting flow curve should be reduced.

For the optimization procedure, the same approach was also used to identify the material parameters of the previous models (El-Magd, Ludwik and Swift) for the extrapolated flow curve.

Table 5 presents a summary of the optimization results obtained for the three behaviour law. The optimal parameters of the behaviour laws for the extrapolated flow curve are reported with the final value of the objective function. It can be noticed that the value of the objective function for El-Magd model is very small (J=13.6) compared to the other values obtained for both Ludwik and Swift models which are 1,883 and 1,514 respectively.

By using these identified parameters, the behaviour laws related to the three studied models were compared to the experimental extrapolated flow curve in Fig. 11. It can be observed that El-Magd model give a very good
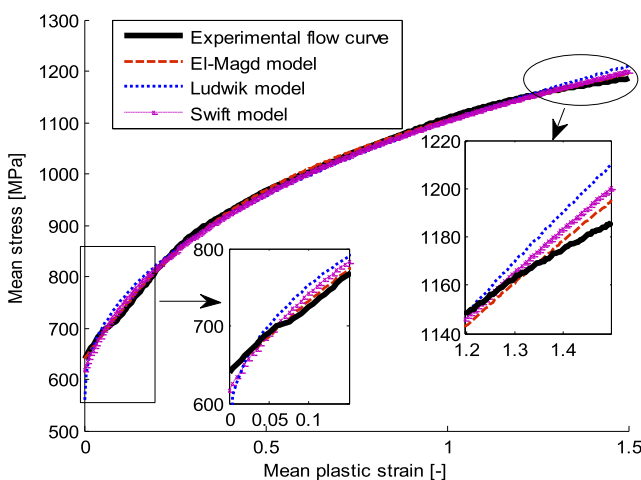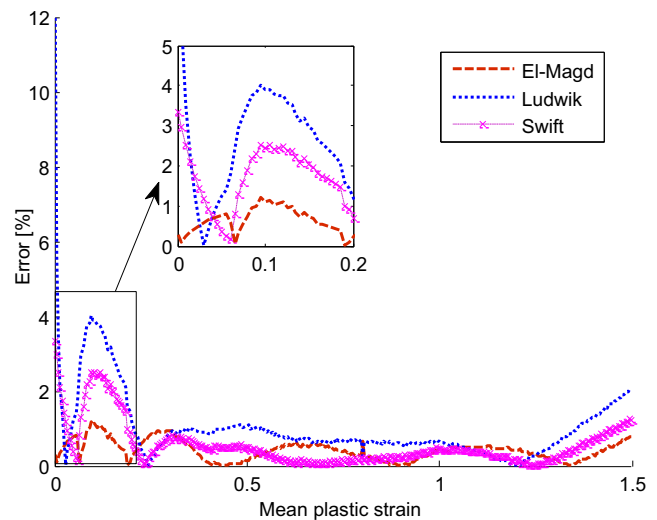

Fig. 9 Error between identified models (El-Magd, Ludwik and Swift) and experimental flow curve for steel 100Cr6

correlation over the model and this is for both flow curve i.e. experimental flow curve limited to εp=1.5 and extrapolated one (extended beyond the limit of εp=1.5). For the other models and with the hypotheses of extrapolated flow curve presented in [22, 23] it can be observed that Ludwik and Swift models do not saturate and give a poor correlation compared to El-magd. Figure 12 illustrates the relative error between extrapolated experimental flow curve and the three models, for Swift and Ludwik model the relative error is about 5 % except at low values of true strain φ, it can reach 10 %. Since the Ludwik and Swift model is only based on a potential term, it is not possible to have good results for both hardening and satiated parts of the flow curve. With the El-Magd model, a good correlation over the whole domain of true plastic strain is achieved and the flow curve is modelled with a relative error under 1.5 %.

FE simulation: identification of the friction coefficient

Numerical identification of the friction coefficient using axial upsetting tests

In order to identify the friction coefficient, a finite element simulation is conducted with the identified material parameters (cf section 4). A sensitivity study on the friction coefficient is performed comparing the numerical curves (force) with experimental ones obtained from the upsetting tests (cf section (Fig. 4).

The 3D finite element model is created using Abaqus 6.11 [18]. The velocity of the upper tool is calculated so that the

Fig. 8 Comparison between identified models (El-Magd, Ludwik and Swift) and experimental curve for steel 100Cr6

Fig. 10 Extrapolation of the
frictionless flow curve to higher
values of true plastic strain
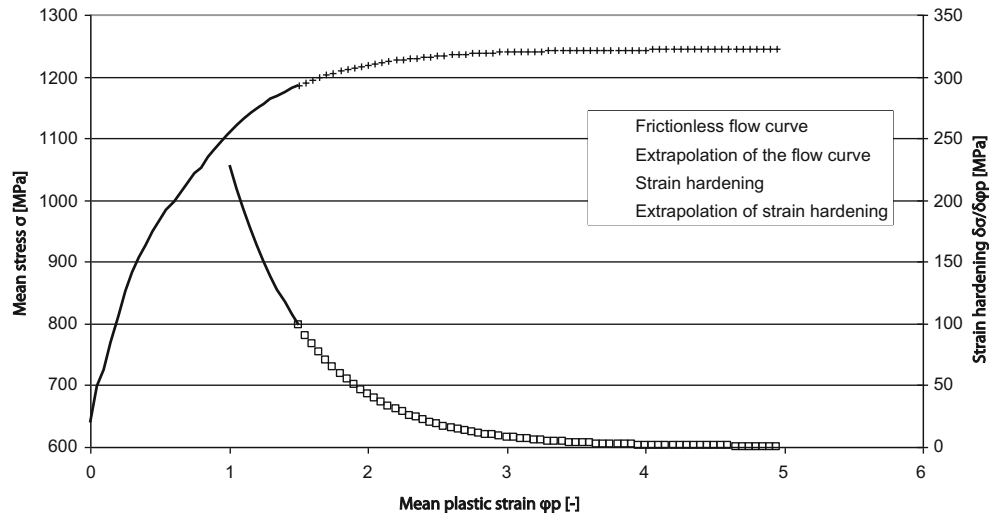
Table 5 Optimization results
with extrapolated flow curve
for El Magd, Ludwik, and
Swift models

Variables	C_1	C_2	C_3	C_4	n	J
El-Magd	632	−4.89	634	0.76	0.87	13.36
Ludiwik	289	781	–	–	0.167	1883
Swift	1072	0.003	–	–	0.124	1514
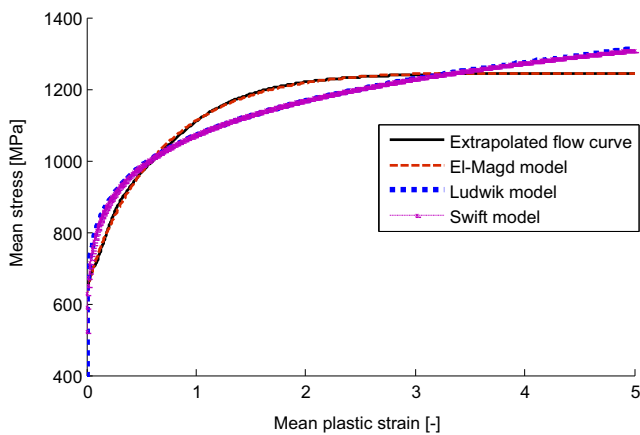
Fig. 11 Comparison between identified models (El-Magd, Ludwik and
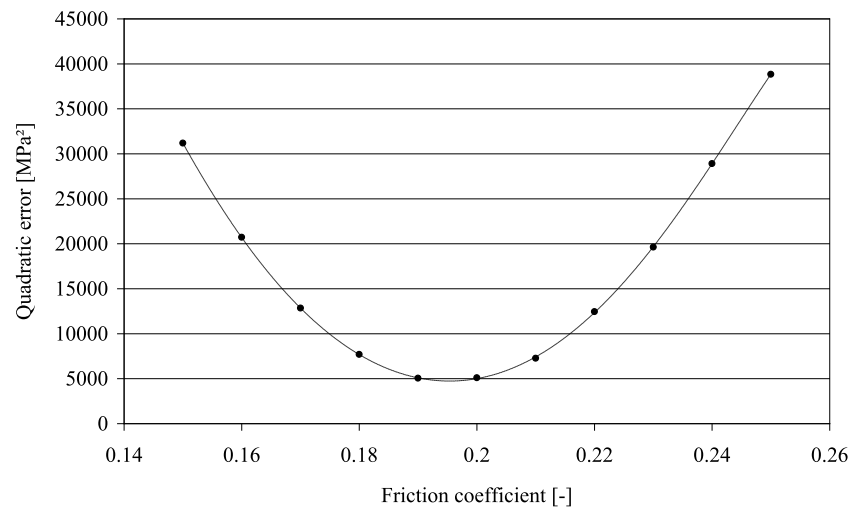Swift) and extrapolated flow curve
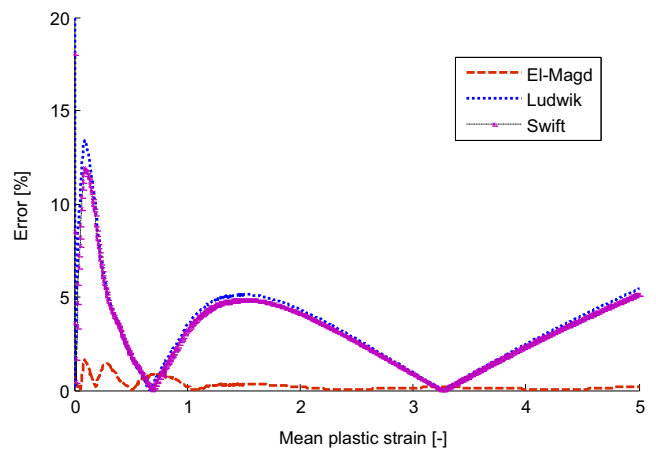
Fig. 12 Error between identified models (El-Magd, Ludwik and Swift)
and extrapolated flow curve

Fig. 13 Identification of thefriction coefficient for steel 100Cr6

global strain rate of the specimen is equal to the one used for the material calibration. Inertial effects are neglected. Accounting for the symmetry of the specimen only one half of the specimen is modelled. The mesh is built using 8-node hexahedral elements with reduced integration, distortion control and hourglass control. 16,250 elements and 18,258 nodes using a global line seed of 0.40 mm are used. The tool is modelled as a rigid body.

The contact between the rigid tool and the sample was modelled with a penalty-controlled surface-to-surface explicit contact. Coulomb's friction law is used for the calculation. The tangential behaviour on the interface was defined with a penalty friction formulation.

The friction coefficient μ of this model was identified using an inverse analysis method. The identification process was performed by using the quadratic error between experimental and numerical curves for different friction coefficients varying from 0.15 to 0.25. Figure 13 illustrates the sensitivity study. A value of 0.195 gives the best value which minimizes this difference.

Modelling of the side pressing test

In the last paragraphs a flow stress model was picked and calibrated using an extrapolation of flow curves from upsetting tests of cylinders with different upsetting ratios. In order to validate the capabilities of the model and the relevance of the material parameters and friction coefficient identification, another finite element analysis was conducted in order to replicate the side pressing test, with the aim of comparing experimental data to the obtained numerical results as illustrated in Fig. 14.

The experimental protocol used to conduct the comparison was the side pressing test. This experimental configuration is a radial compression of a cylindrical specimen.

The experimental protocol for the radial compression test is similar to the axial test described in Fig. 4. The specimen used for the side pressing is the D 10 × H 20 mm one.

In addition to the axial test which allow conducting the material parameters identification, the new configuration of
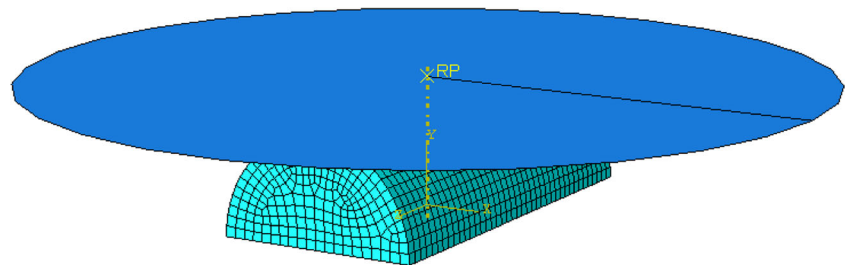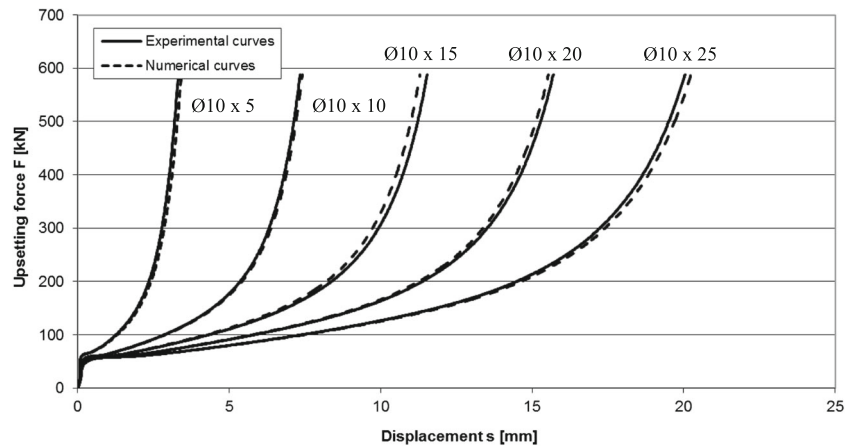
Fig. 14 FE-Model of the side pressing test

the radial compression allowed providing new data to validate the FE model,

Validation of the model and discussion

Both mechanical parameters of the constitutive laws and friction coefficient were identified in order to minimize the error between experimental data and numerical simulations using a given configuration of test (axial tests). Mechanical parameters were identified using an optimization algorithm, and friction coefficient was identified using FE simulation

In order to validate the models as well as the friction coefficient, a second configuration of the test was used: five side pressing tests were simulated using the same friction coefficient, and the predicted forces were compared to the

experimental ones. On Figure15, the predictions of the cylindrical upsetting tests with the identified friction coefficient and identified mechanical parameters are presented. An excellent correlation was observed between experimental data and numerical simulation. It can be seen in Fig. 15, that the force vs. displacement curves perfectly fit experimental data for the five tested samples.

This correlation demonstrates the efficiency of the El-Magd law and its capability to model large deformations problems corresponding to forming processes such as forging or stamping. The identified friction coefficient is also validated.

In terms of shape of the sample, Fig. 16 also illustrates a comparison between experimental results and FE simulation. With the identified friction parameter and constitutive law, good correlation was found between experimental and numerical results in terms shape (radial and axial deformation).
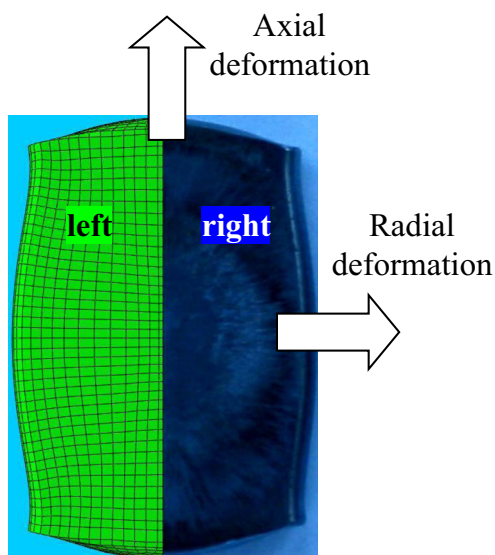
Conclusion

In this paper an identification method for an extrapolated flow curve at large strains is proposed for high strength steel. The approach is based on several points:

– Use of upsetting tests to acquire experimental data for large strains
– Use of different specimens to extrapolate the behaviour to a "frictionless" state
– Use of adequate material model and parameter identification procedure
– Implementation of the identified parameters in a FE code in order to find the appropriate friction coefficient with sensitivity study.
– Validation of the constitutive law and friction coefficient with finite element simulation by comparison with experimental side pressing test.

Fig. 16 Comparison between numerical (*left*) and experimental (*right*) deformed geometry for steel 100Cr6

In the case of the steel 1.3505 the method was used with a flow stress model adapted for large strains and an identification procedure based on a reduced dimension of the identification problem. The identified parameters were implemented in a FE code in order to find the friction coefficient which minimized the quadratic error between experimental and numerical results of upsetting test.

Side pressing tests were also conducted at an experimental level. Based on this configuration of test, the identified model (El-Magd) with the identified friction coefficient were implemented in a FE code and a numerical replication of the side pressing test was performed. Numerical Results in terms of shape of the sample and force/displacement curves were compared to experimental data showing excellent correlations, even if further improvements of the model could be conducted by including the strain rate dependency and the thermal effects.

Finally, the optimal mechanical parameters being identified with different methods, the study provides efficient methodology for the investigation of bulk metal forming.

References

1. Rusinek A, Rodrigues J, Arias A (2010) A thermo-viscoplastic model for FCC metals with application to OFHC copper. Int J Mech Sci 52:120–135
2. Lin YC, Chen XM (2011) A critical review of experimental results and constitutive descriptions for metals. Mat Design 32:1733–1759
3. K. Dahmen, W. Bleck, B. Reichert, Untersuchung der Vorhersagegenauigkeit empirischer Modelle zur Beschreibung des Werkstoffsverhaltens über große Dehnratebereiche, LS-Dyna Forum (2010) 33–40
4. Bonora N, Ruggiero A, Flater PJ, House JW, DeAngelis RJ (2005) On the role of material post-necking stress–strain curve in the simulation of dynamic impact. AIP Conference Proceedings 845:701–704
5. X. Lemoine, A. Lancu, G. Ferron, Flow curve determination at large plastic strain levels: limitations of the membrane theory in the analysis of the hydraulic bulge test, The 14th International Esaform Conference on Material Forming (2011) 1411–1416
6. Parteder E, Büten R (1998) Determination of flow curves by means of a compression test under sticking friction conditions using an iterative finite-element procedure. J Mater Process Tech 74:227–233
7. Jaspers SPFC, Dautzenberg J (2002) Material behaviour in conditions similar to metal cutting: flow stress in the primary shear zone. J Mater Process Tech 122:322–330
8. F. Hahn, Untersuchung des zyklisch plastischen Werkstoffverhaltens unter umformnahen Bedingungen, Ph. D. Thesis, Fakultät für Maschinenbau, Universität Chemnitz, 2003
9. Cook M, Larke EC (1945) Resistance of copper and copper alloys to homogeneous deformation in compression. J Inst Metals 71:371–390
10. Han H (2002) The validity of mathematical models evaluated by two-specimen method under the unknown coefficient of friction and flow stress. J Mater Process Tech 122:386–396
11. Lebaal N, Puissant S, Schmidt FM (2005) Rheological parameters identification using in situ experimental data of a flat die extrusion. J Mater Process Tech 164–165:1524–1529
12. Kim N, Choi H (2008) The prediction of deformation behavior and interfacial friction under hot working conditions using inverse analysis. J Mater Process Tech 208:211–221
13. Guzman R, Melendez J, Zahr J, Perez-Castellanos J (2010) Determination of the constitutive relation parameters of a metallic material by measurement of temperature increment in compressive dynamic tests. Exp Mech 50:389–398
14. Ludwik P (1909) Über den einfluss der deformationsgeschwindigkeit bei bleibenden deformationen mit besonderer berücksichtigung der nebenwirkungserscheinungen. Physikalisch Zeitschrift 10:411–417
15. Swift MW (1952) Plastic instability under plane stress. J Mech Phys Solid 1:1–18
16. E. El-Magd, In: G.E. Totten L. Xie, K. Funatani, Modeling and simulation for material selection and mechanical design, Marcel Dekker, Inc., (2004) 195–300
17. Harb N, Labed N, Domaszewski M, Peyraut F (2011) A new parameter identification method of soft biological tissue combining genetic algorithm with analytical optimization. Comput Methods Appl Mech Eng 200:208–215
18. Dassault Systèmes, Abaqus 6.11 Theory Manual, Providence, 2011
19. Ansys Inc., Theory reference for Ansys, Canonsburg, 2011
20. LSTC, LS-Dyna Keyword user's manual, Livermore, 2007
21. Johnson GR, Cook WH (1983) A constitutive model and data for metals subjected to large strains, high strain rates and high temperatures, Proc, 7th Int. Symp. Ballistics, Netherlands, 541–547
22. T. Emde, Mechanisches Verhalten metallischer Werkstoffe über weite Bereiche der Dehnung, der Dehnrate und der Temperatur, Ph.D. Thesis, Fakultät für Maschinenwesen, Universität Aachen, 2008
23. Voce E (1948) The relationship between stress and strain for homogeneous. J Inst Met 74:537–562
24. Poulachon G, Moisan A, Jawahir IS (2001) On modelling the influence of thermo-mechanical behavior in chip formation during hard turning of 100Cr6 bearing steel. Annals of CIRP 50:31–36
25. Taylor GI, Quinney MA (1934) The latent heat remaining in a metal after cold work. Proc Roy Soc A 143:307–326
26. Zehnder A, Babinsky E, Palmer T (1998) Hybrid method for determining the fraction of plastic work converted into heat. Exp Mech 38:295–302
27. Meyer LW, Herzig N, Halle T, Krueger L, Staudhammer KP (2007) A basic approach for strain rate dependent energy conversion including heat transfer effects: An experimental and numerical study. J Mater Process Tech 182:319–326
28. Toussaint L, Lebaal N, Schlegel D, Gomes S (2011) Automatic optimization of Air conduct design using experimental data and numerical results. Int J Simul Multidisci Des Optim 4:77–83
29. Lebaal N, Puissant S, Schmidt F (2010) Application of a response surface method to the optimal design of the wall temperature profiles in extrusion die. Int J Mater Form 3:47–58